ELSEVIER

Synthetic Metals 78 (1996) 253–261

SYNTHETIC METALS

Poly(*p*-pyridine)- and poly(*p*-pyridyl vinylene)-based polymers: their photophysics and application to SCALE devices

A.J. Epstein [a,b,c], J.W. Blatchford [a], Y.Z. Wang [a], S.W. Jessen [a], D.D. Gebler [a], L.B. Lin [c], T.L. Gustafson [b,c], H.-L. Wang [d], Y.W. Park [d], T.M. Swager [d], A.G. MacDiarmid [d]

[a] *Department of Physics, The Ohio State University, Columbus, OH 43210-1106, USA*
[b] *Department of Chemistry, The Ohio State University, Columbus, OH 43210-1106, USA*
[c] *Chemical Physics Program, The Ohio State University, Columbus, OH 43210-1106, USA*
[d] *Department of Chemistry, University of Pennsylvania, Philadelphia, PA 19104-6323, USA*

Received 15 January 1996

Abstract

Photophysics and light-emitting device applications of poly(*p*-pyridine)- and poly(*p*-pyridyl vinylene)-based polymers are presented. Extensive time-resolved (ps to ms) photoluminescence, stimulated emission and photoinduced absorption studies of solutions, powders and films demonstrate that the primary photoexcitation of these polymers is an intrachain singlet exciton. The presence of (n,π^*) states leads to enhanced intersystem crossing to triplet excitons for the powder form, while aggregate formation plays a key role in the films. Polarons are important at longer times. These polymers were used to fabricate 'conventional' polymer light-emitting diodes. In addition, these polymers were used to demonstrate a novel light-emitting structure, the symmetrically configured a.c. light-emitting (SCALE) device. These new devices have potential advantages in their use with high workfunction electrodes, such as gold, and also in their a.c. operation.

Keywords: Poly(*p*-pyridine); Poly(*p*-pyridyl vinylene); Photophysics; SCALE devices

1. Introduction

Recently, there has been extensive interest in understanding the electronic ground state and the excitations of C_6 ring-containing polymers, especially poly(*p*-phenylene vinylene) (PPV) and poly(*p*-phenylene) (PPP). The effects of Coulomb interaction, electron–phonon interaction and interchain interaction (including polymer chain conformations) in determining the stable charge and neutral excitations of the semiconducting polymers are under investigation. Establishment of the roles for neutral singlet and triplet excitons and charged polarons and bipolarons is important for the fundamental science of this class of materials, and for their potential applications for devices such as light-emitting diodes (LEDs) and symmetrically configured alternating current light-emitting devices (SCALE devices). Though significant progress has been made in determining the role of excitons and polarons in PPV and PPP, important controversies remain. Similarly, though there have been dramatic advances in the brightness and lifetimes of LEDs prepared utilizing PPV and PPP and their derivatives, important problems remain to be resolved before widespread commercial application is feasible [1].

Here we present results of a study of nitrogen derivatives of PPP and PPV, that is, poly(*p*-pyridine) (PPy) and poly(*p*-pyridyl vinylene) (PPyV) (see Fig. 1). These materials differ electronically from PPP and PPV in that they contain a nitrogen atom in the six-membered ring replacing a CH group in the *ortho* or *meta* position. The presence of the nitrogen atoms introduces two important advantages: (1) the charge conjugation symmetry of the PPP and PPV systems is now broken, allowing one to probe the relative importance of Coulomb interaction and electron–phonon interaction; (2) the presence of the N group with its lone pair of sp^2 electrons enables processing of the PPy and PPyV polymers so that they can be studied in a wide variety of forms, including protonated at the N site in solution in formic acid, as powders precipitated from *N*-methylpyrrolidinone (NMP), and as spin-cast or drop-cast films prepared from formic acid. Generally there is no signature that formic acid remains, so that the resulting films are unprotonated.

We have carried out photoinduced absorption (PA), stimulated emission (SE) and time-resolved photoluminescence (PL) studies of these polymers on a wide variety of time scales ranging from picosecond through to seconds for materials in the form of solution, powders and films. By consid-

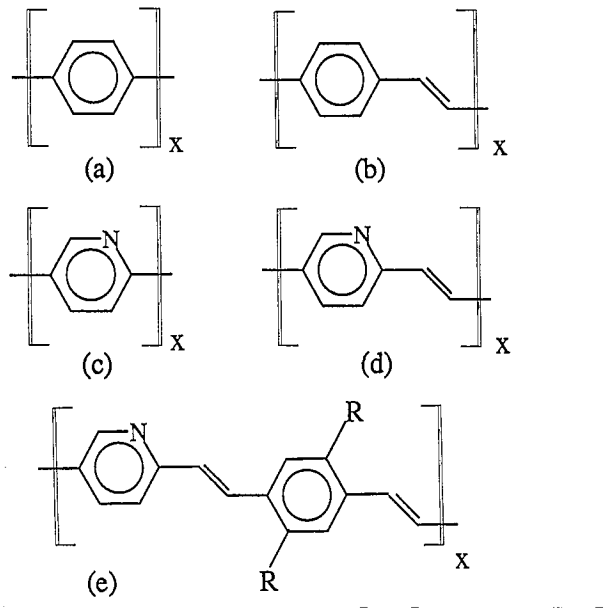

Fig. 1. Repeat units for (a) poly(*p*-phenylene) (PPP), (b) poly(*p*-phenylene vinylene) (PPV), (c) poly(*p*-pyridine) (PPy), (d) poly(*p*-pyridyl vinylene) (PPyV), and (e) copolymers of PPyV and PPV derivatives.

ering the evolution of the PA, SE and PL at ps and ns times as PPyV samples are processed, we conclude that, in all three morphologies of this polymer, the PA at early times is due to intrachain singlet excitons, the same species that give the PL. Furthermore, we observe a second, long-lived component of the PA which we demonstrate originates from triplet excitons created via intersystem crossing between the singlet and triplet manifolds. The observation of the triplet signal is suggested due to the result of the effects of the non-bonding states associated with the nitrogen atoms present in the conjugated backbone of PPyV which are not present in phenylene-based polymers such as PPV. Similar results are also obtained for the PPy-based polymers.

We have fabricated LEDs from PPy and PPyV. Though their electroluminescence (EL) efficiencies as yet are modest, these easily processed polymers are potentially a basis of fabricating a range of LEDs of colors varying from orange through blue. Recently, we have utilized these materials and related copolymer poly(phenylene vinylene pyridyl vinylene) to prepare a new type of light-emitting device, the SCALE device. In these latter devices, 'insulating' layers of an electroactive polymer such as emeraldine base (EB) or nonelectroactive polymers such as poly(methyl methacrylate) (PMMA) are added between the light-emitting polymer layer and each of the two electrode layers. The resulting device has lower threshold voltages with higher currents, and, most importantly, operates equally well in forward and reverse, nearly independently of the workfunction of the electrode contacts. This enables use of high workfunction, noncorroding gold as electrode contact material in these devices.

2. Experimental techniques

The syntheses of PPy [2], PPyV [3], the copolymers [4] of PPyV and PPV polymers and emeraldine base polymer (EB) [5] have been reported earlier. The optical absorption measurements were performed on a Perkin-Elmer Lambda-19 UV–Vis–NIR spectrometer. The fluorescence measurements were recorded on a SPEX Fluorolog flourometer. Millisecond PA measurements used mechanically chopped (4 Hz–4 kHz) excitation from a cw argon laser and a tungsten lamp as a broadband probe. The reported spectra were acquired at 80 K with about 100 mW/cm^2 excitation. Time-resolved fluorescence measurements involved excitation at 1 MHz from a Coherent 700 series cavity-dumped synchronously pumped dye laser and utilized the time-correlated single-photon counting technique (about 50 ps resolution). Picosecond PA was detected with a second Coherent dye laser, giving about 10 ps resolution. The time-resolved measurements were performed at room temperature and excited with 2 nJ pulses at 2.8 eV.

For these measurements, powder samples were dispersed in KBr and pressed into 0.02% pellets. Powders were also dissolved in formic acid (HCOOH) for solution study. Film samples were prepared by spinning or dropping concentrated solutions (about 10 mg/ml) onto quartz substrates. Note that, while the powder samples were stored in an inert environment, the film samples were prepared under ambient conditions.

Quantum chemical calculations were performed with commercially available software. The PM3 technique was used to optimize the geometries of various model oligomers, and absorption spectra were calculated using single-excitation configuration interaction.

The electroluminescent device fabrication procedures can be found in other reports [6]. PPy and PPyV films were spun-cast from formic acid while the films of EB and the copolymer were spun-cast from NMP and xylene, respectively. PL and EL were measured using a PTI fluorometer (model QM-1). The current–voltage (*I–V*) characteristics were measured simultaneously with EL using two Keithley 195A multimeters, while d.c. voltage was applied by a HP 6218A d.c. power supply. Under a.c. driving the sinusoidal voltage was supplied by a HP 3311A function generator. The EL intensity was measured using a photomultiplier (PMT, Hamamatsu Photonics, type R928) and a Tektronix 2430A oscilloscope.

3. Photophysics of pyridine-based polymers

Fig. 2(a) shows the measured optical absorption spectrum of PPyV and PPy films on quartz substrates. The PPyV spectrum displays four peaks, in agreement with recent predictions for systems with broken charge-conjugation symmetry [7] and also the presence of Coulomb interactions [8]. The PPy spectrum shows only two distinct features; however, several unresolved features may be present in the background

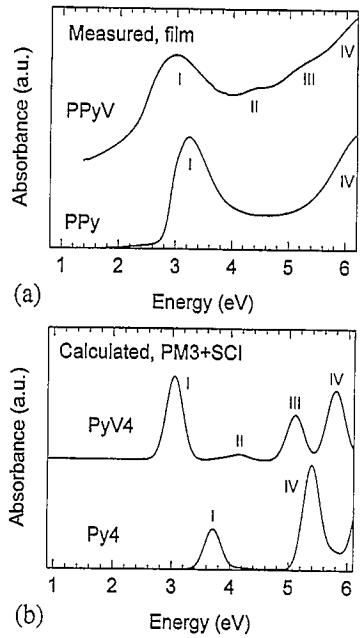

Fig. 2. (a) Measured optical absorption of PPyV and PPy films on quartz. (b) PM3+SCI calculated absorption spectra for four-ring oligomers of PPyV (PyV4) and PPy (Py4). CI space: 15×11 and 12×8, respectively.

between 4 and 5.5 eV. Fig. 2(b) shows the calculated absorption spectra for four-ring oligomers of PPyV (PyV4) and PPy (Py4). While the exact positions of the polymer absorption peaks are not well reproduced (especially in the case of PPy), the 'tetramer' spectra are qualitatively similar to the polymer spectra: the PPyV oligomer shows four prominent peaks, the PPy oligomer only two. While the first transition in each of the tetramer spectra is nearly 100% HOMO to LUMO, the other transitions display strong mixing amongst the various Hartree–Fock bands.

The pyridine-based systems differ from polymers such as PPV and PPP in that they possess additional (n,π^*) states which result from the promotion of a lone-pair electron from the nitrogen heteroatom to the π^* backbone. The quantum chemical calculations also indicate that the lowest (n,π^*) states should be located more than 1 eV above the lowest singlet (π,π^*) transitions in the planar polymer. This is an important result, as systems where an (n,π^*) state lies below the lowest (π,π^*) singlet generally display only weak luminescence, as intersystem crossing between (n,π^*) and (π,π^*) states is allowed to first order in the spin–orbit interaction [9]. A dramatic example is pyridine itself, which shows no detectable luminescence.

The first absorption band for the film, solution and solid samples of both polymers is shown in Fig. 3. All spectra have broad features, suggesting a distribution of conjugation lengths and ring-torsional ground states. In both cases the powder absorption spectrum is nearly identical to the solution spectrum. In contrast, the film spectra as compared with solution spectra show evidence for extra oscillator strength at low energies. The PL spectra for each of the three forms of the two polymers are shown in Fig. 4. Again, the powder and

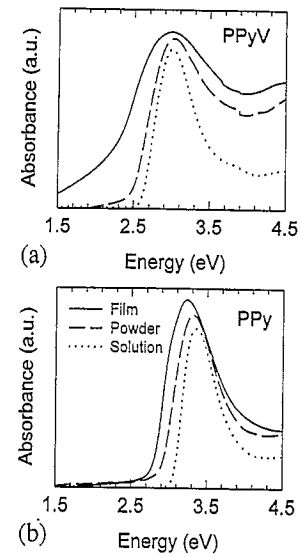

Fig. 3. Measured optical absorption spectra for (a) PPyV and (b) PPy solutions in HCOOH (dotted), powders in KBr (dashed) and films on quartz (solid).

solution spectra are quite similar, and are in fact identical when self-absorption effects are taken into account. The film spectrum, however, is strongly red-shifted. Additionally, the PL excitation spectra (not shown) for the film samples are also red-shifted versus the solution samples. In conjunction with the change in the optical spectrum presented above, these results argue for the presence of additional low-energy emitting states in these systems.

We suggest that these low-energy states are aggregate sites, where the ground-state and excited-state wavefunctions can delocalize over several chains [10,11]. The formation of aggregates has been recently suggested to occur in ladder-like PPP analogues [12]. In support of a morphology-

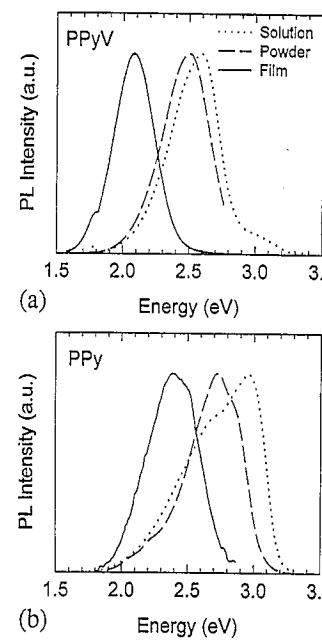

Fig. 4. PL spectra of (a) PPyV and (b) PPy solutions in HCOOH (dotted), powders in KBr (dashed) and films on quartz (solid).

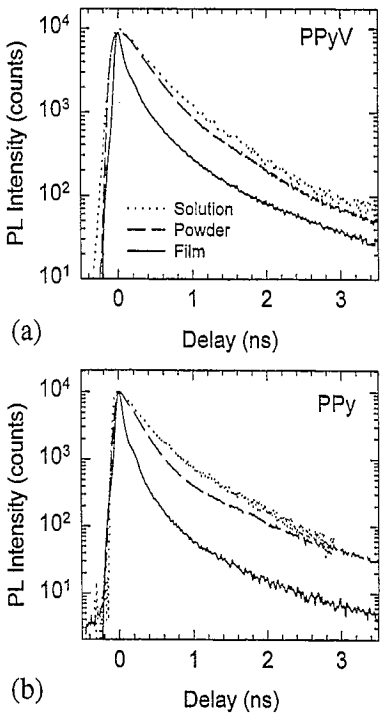

Fig. 5. PL decay of (a) PPyV and (b) PPy solutions in HCOOH (dotted), powders in KBr (dashed) and films on quartz (solid).

dependent mechanism such as aggregate formation, the red shift in film emission is observed to be dependent on the solvent from which the film is cast. Moreover, the aggregates evidently do not form in powder samples, which preliminary X-ray diffraction measurements [13] demonstrate to be more disordered than film samples. The formation of luminescent aggregates in PPyV is now confirmed in near-field scanning optical microscopy studies [14].

The formation of aggregates has a strong effect on the PL dynamics as well. This is demonstrated in Fig. 5, where the PL decays are shown for all morphologies of both polymers. The powder and film samples show strong spectral diffusion (PL decay depends on wavelength); therefore, the PL decays shown are numerically integrated over energy, and thus represent the decay of the total exciton population. The powder decay closely follows that of the solution decay, indicating that spectral diffusion in powder samples is due to exciton migration. On the other hand, the film samples initially show a reduction in PL lifetime, corresponding to emission from intrachain excitons, followed by a slow component, ascribed to aggregate emission.

The reduction in PL intensity evident in Fig. 5 is matched by the reduction in internal quantum efficiency. For PPyV, the solution decay corresponds to a quantum efficiency of 22% (versus a Rhodamine standard). The internal quantum efficiency predicted for the film, found by comparing the integrated area under the PL decay to that of the solution, is about 10%. The measured external quantum efficiency for the film PL is 3%. For a refractive index of 1.9 (from Kramers–Kronig analysis of the reflection spectrum) the measured internal quantum efficiency of the film is 11%, in close agreement with that predicted from the PL decay. This result argues strongly against direct photogeneration of competing species such as 'polaron pairs' [15] in our samples. The reduced efficiency of our samples is accounted for by an increase in nonradiative decay.

We now consider the results of our PA studies. The PA spectra at 0 ps (with 10 ps resolution) and at ms time scales are shown for both polymers in powder form in Fig. 6. We demonstrate below that the 0 ps spectrum represents a singlet–singlet transition. The cross section for this transition is extremely large (on the order of the ground-state cross section), reminiscent of earlier observations for *trans*-stilbene [16]. The 0 ps PA spectrum is approximately the same in all forms for both polymers. In addition to PA, in PPyV powders and solutions stimulated emission (SE) is observed at the edge of the detection window (2.2 eV), as is evidenced by the negative signal at this energy. For solution samples, we have extended the probe range to 3.8 eV using broadband femtosecond PA measurements, and we observe stimulated emission across the entire PL spectrum in both polymers [10,11]. In contrast, no stimulated emission is seen below 2.2 eV in films, which we ascribe to strong absorption and scattering at these wavelengths due to the aggregate sites.

The ms PA feature corresponds to a triplet–triplet transition [13] in both polymers, as is evidenced by its linear intensity dependence and monomolecular decay dynamics. In addition, optically detected magnetic resonance experiments confirm the presence of triplets in the powder samples [17]. Unlike the ps PA spectrum, the ms PA spectrum is strongly dependent on morphology, as is demonstrated for PPyV in Fig. 7. The film spectrum shows a two-peaked feature which has sublinear intensity dependence, power-law decay kinetics

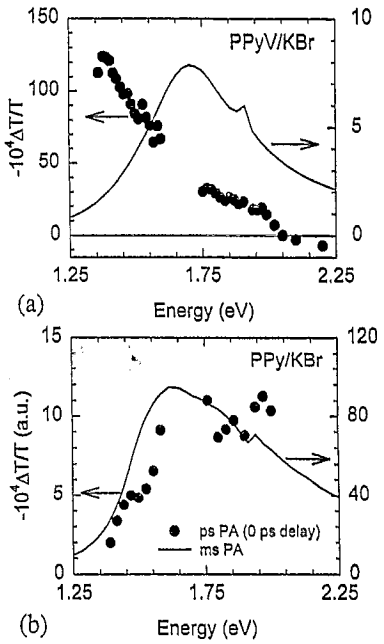

Fig. 6. Picosecond PA spectra at 0 ps delay with 10 ps resolution (circles) and millisecond PA spectra (solid line) for (a) PPyV and (b) PPy powder in KBr.

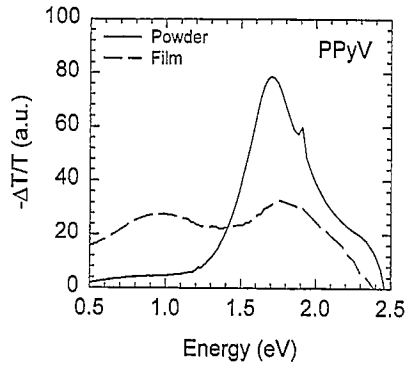

Fig. 7. Millisecond PA spectra for PPyV powder in KBr (solid) and film on quartz (dashed).

and accompanying infrared-active vibrations. We assign this feature to polaron absorption. The persistence of a two-feature polaron spectrum, despite the breaking of inversion symmetry due to the nitrogen heteroatom, is also borne out in our quantum chemical calculations [11]. We argue below that the difference in the powder and film spectra is due to enhanced intersystem crossing in the powder samples.

The dynamics of the ps PA are compared with those of the PL for all three morphologies of PPyV in Fig. 8. The results for PPy are similar, though they are not presented here. In solution (Fig. 8(a)), the PA at 1.4 eV (the peak of the ps PA band) closely follows the PL decay, indicating that the PA band originates from singlet excitons. At 1.9 eV, an additional long-lived PA is evident. The contribution of the long-lived state is independent of solution concentration, and we therefore suggest its origin to be triplet excitons.

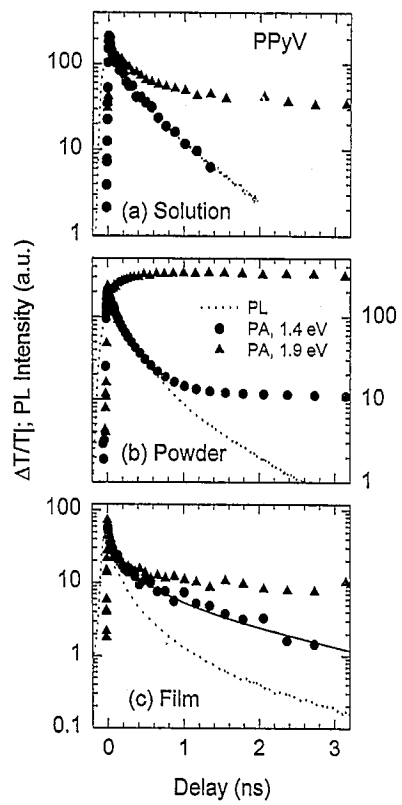

Fig. 8. Picosecond PA decay at 1.4 eV (circles), at 1.9 eV (triangles) and energy-integrated photoluminescence decay (dotted lines) for (a) PPyV in HCOOH, (b) PPyV powder in KBr, and (c) PPyV film on quartz. Solid line in (c) is the exciton density obtained from the PL decay.

Further evidence for this assignment is found in Fig. 8(b). Again, the PA decay at 1.4 eV closely follows the PL at early times, suggesting that the PA is due to a singlet–singlet transition in powder samples as well. After about 1 ns, however, the PA at 1.4 eV is dominated by a long-lived signal, similar to that seen at 1.9 eV in the solution. The powder PA decay at 1.9 eV is entirely dominated by this long-lived state, and a definite rise to the long-lived response is noticeable. The rise of the long-lived state nearly exactly matches the decay of the PA due to singlet excitons. The spectral response of the PA at 1 ns identifies the long-lived state as a triplet exciton in these samples. The linear intensity dependence, the correlation of the rise of the long-lived state with the decay of the singlet and a pump wavelength dependence that follows the PL excitation spectrum demonstrate that the triplets are produced by direct intersystem crossing from the singlet manifold, and not by other means, such as singlet–singlet fusion or two-photon absorption. Note that triplet generation in solutions is about 10 times smaller than in powders, a point to which we return below.

The dynamics of the film PA are shown in Fig. 8(c). In this case, the PL dynamics are highly non-exponential, and the PA and PL cannot be expected to have the same relationship as in solution. If the quantum efficiency for emission is approximately independent of time, then the PL is proportional to the rate of change of the exciton density, dn/dt. On the other hand, the PA is directly proportional to the exciton density, n, leading to the relationship $PL \sim d(PA)/dt$ [18,19]. Indeed, this is what is seen in PPyV films for the PA at 1.4 eV. The solid line in the figure represents the exciton density obtained by fitting the PL decay and integrating the fit analytically. The close agreement between the PA and the exciton density indicates that the early PA is due to singlet excitons in film samples, as well as in solutions and powders. Again, this observation argues against substantial photoproduction of competing species such as 'polaron pairs' [15] in our samples.

The film samples also show evidence for triplet generation, as is evidenced by the PA decay at 1.9 eV. Again, a long-lived state is indicated in the PA at this energy. Note, however, that the contribution of the long-lived state is again 10 times smaller than is observed for the powder samples. The suggested origin of the morphology-dependent intersystem crossing rate is based on our quantum chemical calculations, which demonstrate that strong mixing occurs between (n,π^*) and (π,π^*) states when ring-torsional disorder is introduced into the polymer. In particular, for a PPyV tetramer with a 90° ring torsional defect, a triplet state of strong (n,π^*) character falls below the lowest (π,π^*) singlet, providing an additional route for intersystem crossing. We suggest that our powder samples contain somewhat higher levels of these ring-torsional defects than the films or solutions. This conjecture is consistent with the higher degree of disorder of

the powder samples as detected in X-ray diffraction measurements [13]. As extensive exciton migration is suggested by the spectral diffusion observed in the PL measurements, a small density of ring-torsional defects could very easily lead to a large enhancement in intersystem crossing in these morphologies.

4. Light-emitting devices

We have made light-emitting devices from PPy, PPyV and copolymers of PPV and PPyV. Similar to devices based on PPV and most other electroluminescent conjugated polymers and/or copolymers [20–22], which have been shown to be tunneling diodes [23] and can only operate under forward d.c. driving field, the pyridine-based devices in their simplest sandwich structure also show diode behavior [24]. Fig. 9 shows a typical *I–V* characteristic for such a PPy device in the ITO/PPy/Al configuration. Light is emitted at the same voltage as the current begins to increase rapidly, and then varies with the current. The inset of Fig. 9 shows the *I–V* characteristics on a log–log scale. At low voltages, a power law behavior is observed, $I \sim V^n$, with $n \sim 2$, indicating space-charge limited current transport [25] with $J = (9/8)\epsilon\mu_{\text{eff}}V^2/d^3$. Here ϵ is the dielectric constant, μ_{eff} the effective mobility and d is the thickness of the film. Assuming $\epsilon \sim 4$, from the slope of J versus V^2, we estimate $\mu_{\text{eff}} \sim 10^{-6}$ cm^2/(V s). Similar *I–V* characteristics were observed for PPyV and copolymers of PPyV and PPV. The use of hole-transporting material such as poly(vinylcarbazole) (PVK) and the use of a network electrode such as the emeraldine salt of polyaniline with camphor sulfonic acid as the counterion (PAN-CSA) blended with the emitting polymer [26] improve the device performance dramatically.

There have been some reports of the observation of EL in reverse bias for certain systems in the simple sandwich structure [27–29] and for some multiple bilayer structures prepared by a dip-coating technique [30], although some of these devices show unstable EL and/or need much higher driving voltage under reverse bias. Recently, we have reported the fabrication of SCALE devices based on PPy and PPyV by introducing two insulating (I) layers, such as the emeraldine base (EB) form of polyaniline, sandwiching the emitting layer [6]. The SCALE devices emit light under both forward and reverse d.c. bias, as well as under a.c. driving voltage. This unusual behavior is attributed to the effects of charge accumulation at the polymer/polymer interfaces [6]. The SCALE device structure, ITO/I/emitter/I/M, has been shown to be quite general and can be applied to a variety of electroluminescent polymers (emitter), insulating polymers (I) and electrode materials (M).

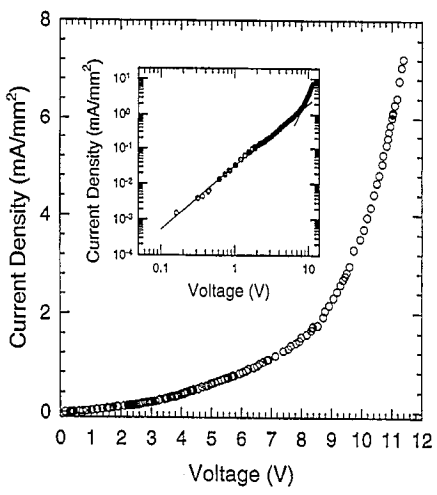

Fig. 9. *I–V* characteristic for a typical ITO/PPy/Al device. Inset: same *I–V* characteristic plotted on a log–log scale.

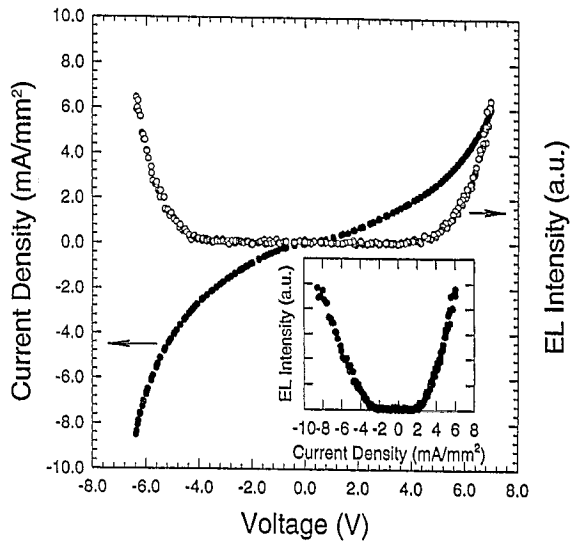

Fig. 10. *I–V–*EL characteristics for the ITO/EB/copolymer/EB/Al device. Inset: EL–*I* characteristic for the same device.

Here we summarize and compare the performance of SCALE devices fabricated with different emitters (e.g. PPy, PPyV and copolymers of PPyV and PPV derivatives (Fig. 1)), insulators (e.g. EB and poly(*o*-toluidine) (POT)), and electrode materials (e.g. Al and Au).

Fig. 10 shows the current–voltage–electroluminescence (*I–V–*EL) characteristics for the ITO/EB/copolymer (R = $COOC_{12}H_{25}$)/EB/Al device. The device emits light symmetrically in both forward and reverse d.c. bias with similar *I–V* and EL–*V* characteristics. Under low frequency a.c. (sinusoidal) driving voltage, light pulses with double the driving frequency were observed. The inset of Fig. 10 shows the EL–*I* characteristics of the device. The EL intensity depends linearly on current in both forward and reverse bias although the EL is slightly more efficient in the forward bias. Similar behaviors are observed for ITO/EB/PPy/EB/Al, ITO/EB/PPyV/EB/Al and ITO/POT/copolymer/POT/Al devices.

Fig. 11 compares the *I–V* characteristics for ITO/EB/PPy/EB/electrode SCALE devices utilizing Al and Au as the top electrode. The two devices emit light under both forward and reverse bias, and show similar *I–V* characteristics with similar turn-on voltages despite the fact that Al and Au have very different workfunctions (4.2 versus 5.3 eV, respec-

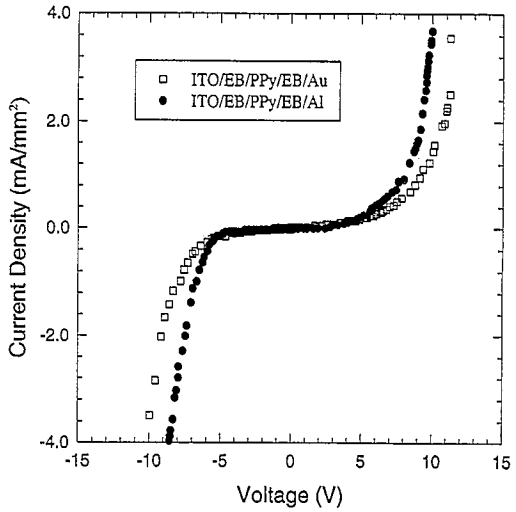

Fig. 11. *I–V* characteristics of ITO/EB/PPy/EB/Al and ITO/EB/PPy/EB/Au devices.

tively) [21]. Note that the thickness of the EB layers in the Au device is thicker than those in the Al device, which may account for the slightly higher threshold voltage for the Au device. (The motivation for thicker EB in the Au device is reduction of diffusion of Au into the emitter layer.) Under low frequency a.c. (sinusoidal) driving voltage, light pulses with twice the driving frequency were observed. Fig. 12 shows the variation of the EL intensity of a ITO/EB/PPy/EB/Al device driven by a 60 Hz sinusoidal voltage. A similar result was observed for ITO/EB/PPy/EB/Au devices.

The charge injection mechanism for polymer LEDs is usually represented by a very simplified model, within which the emitting polymer/electrode interface is assumed to be an abrupt separation between two media with no localized electronic states (interface states). As a consequence, the *I–V* characteristics for most polymer LEDs have been proposed to be controlled by a workfunction-related tunneling mechanism [23]. However, a vast amount of work on semiconductors has shown that it is common that interface states exist at the metal/semiconductor interface [31,32]. The symmetric *I–V* curves, which are not sensitive to the electrode workfunction for the SCALE devices, suggest that interfaces play an important role in the device operation. The introduction of the EB layers into the device dramatically changes the distribution of charge injection barriers.

To study the role of the EB layer in the SCALE device operation, we fabricated the following device structures: ITO/PPy/Al, ITO/EB/PPy/Al, ITO/PPy/EB/Al, ITO/EB/PPy/EB/Al and ITO/EB/Al. Fig. 13 compares the *I–V* characteristics for these devices. The light intensity follows closely with the corresponding *I–V* curve, except for the ITO/PPy/EB/Al device in reverse bias, in which case no light was observed although there was significant current flow. It is noted that the turn-on voltage for the multilayer device ITO/EB/PPy/EB/Al is lower than the corresponding single layer device ITO/PPy/Al with the same thickness of the PPy layer, despite the extra thickness of EB layers. The unusual behavior suggests that charge injection from either metal electrode through EB to PPy is easier than to PPy directly. Similar behavior has been observed for the SCALE devices based on other polymer systems when EB is used as the insulating polymer [33]. This behavior is attributed to EB being a redox polymer, able to accept electrons or holes easily to vary its oxidation states reversibly. The nearly linear *I–V* characteristic for the ITO/EB/Al structure under low forward and reverse bias voltages (Fig. 13 inset) suggests that very small, if any, barriers exist in the EB/electrode interfaces.

The available negative and positive polaron levels within the emeraldine base polymer band gap may play an important role in charge injection and transport. Specifically, under low bias voltages, electrons and holes can be injected from the electrodes to the quinoid and benzenoid levels of EB and form negative and positive polarons, respectively. Because the polarons levels are within the band gap of EB, and are

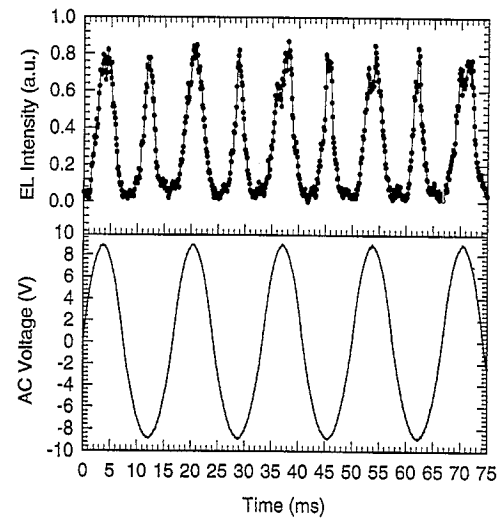

Fig. 12. A.c. response of a SCALE device ITO/EB/PPy/EB/Al driven by a 60 Hz sinusoidal voltage.

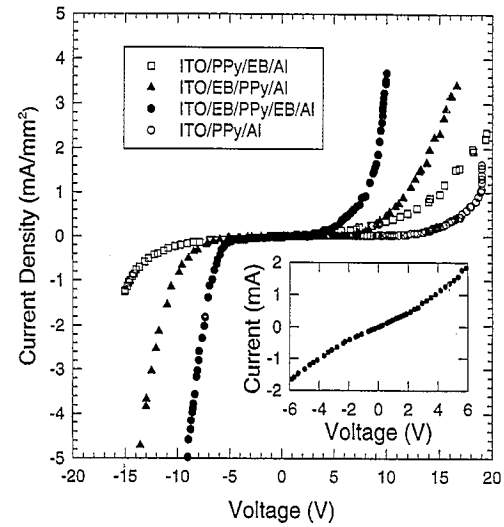

Fig. 13. *I–V* characteristics of four devices with different structures as shown in the figure. Note that the turn-on voltage decreases as the total number of layers increases. Inset: *I–V* characteristic for the ITO/EB/Al structure.

also likely within the band gap of PPy, the barriers for charge injection from electrodes to polaron levels of EB are significantly reduced as compared to injection directly to conduction and valence bands of PPy. Within this model, the limiting barriers for charge injection are changed from the electrode/polymer contacts as proposed for conventional polymer LEDs to the polymer/polymer (EB/PPy) interfaces of the SCALE devices.

We point out that the significant reduction of barrier height at the electrode/EB interface enables the use of stable high workfunction metals (such as Au) as electrodes, which reduces the problems of aging of contacts in polymer light-emitting devices. Due to the inter-penetrating network nature of the polymer/polymer interfaces, non-uniform electric fields may be created facilitating charge injection and, hence, reducing the effective barrier. This non-uniform electric field effect was demonstrated in PPV devices using high-surface area network conducting polyaniline as the hole injection electrode [34].

While ITO/EB/PPy/EB/Al and ITO/EB/PPy/Al devices emit light in both forward and reverse bias, no light (or very weak light) was observed for ITO/PPy/Al and ITO/PPy/EB/Al devices under reverse bias, indicating that electron injection from ITO to PPy is the main efficiency limiting step in the device operation under reverse bias. The current flow in the ITO/PPy/EB/Al is essentially hole current under reverse bias. By adding the EB layer in between ITO and PPy, however, the electrons are able to inject into PPy through EB, and recombine with holes injected from the Al electrode through the EB layer. Therefore, emission can be observed in ITO/EB/PPy/EB/Al devices under reverse bias. The fact that light was also observed at higher voltage for the ITO/EB/PPy/Al device under reverse bias indicates that holes can be injected from Al into PPy at high enough field, probably due to the existence of a thin Al_2O_3 oxide layer.

We propose the following mechanism for the SCALE device operation [6]. Under low bias voltage, electrons and holes are injected from the electrodes to the gap states of EB and form negative and positive polarons, respectively. These polarons transport to the EB/PPy interfaces via a hopping mechanism and populate the EB/PPy interfaces. When the applied electric field is high enough, the stored charges begin to tunnel into the conduction and valence bands of PPy. When they meet, the injected charges may form intrachain excitons and decay radiatively to emit photons or follow other non-radiative decay paths. If the charge injection is not balanced, as is the case for most polymer LEDs, the excess charge carriers may migrate through the PPy layer without decaying. Most of these charges may be trapped in interface states at the opposite PPy/EB interface. When the bias voltage is reversed, the shallow trapped charges will be released from the interface states and contribute to the recombination current. The deep trapped charges which act as quenchers or injection limiters in d.c. devices will be neutralized. We point out that the use of stable high workfunction metals, such as Au, as electrodes to inject both electrons and holes for the SCALE devices may reduce the problems of aging of contacts of polymer light-emitting devices. Also, continuous reversal of the sign of the driving voltage under a.c. operation may reduce degradation.

The SCALE devices have a number of potential advantages over the 'conventional' polymer LEDs:

(1) The limiting barriers for charge injection are moved from the electrode/polymer interfaces (where the barriers are difficult to reduce and control) to the redox polymer/emissive polymer interfaces, which dramatically reduces the overall charge injection barriers, thereby lowering operating voltages, and allows control using a full range of organic/polymer chemistry. This could lead to significant improvement in charge injection efficiency by choosing appropriate redox polymers.

(2) The charge injection from the electrodes to the redox polymer is nearly ohmic for a variety of metals. Thus, the SCALE device performance is not sensitive to the electrode materials used. This enables the utilization of stable high workfunction metals (including gold) as an electrode, potentially reducing the aging problems associated with 'conventional' polymer LEDs which must use reactive low workfunction metals to achieve efficient electron injection.

(3) The SCALE devices can operate equally well under both forward and reverse d.c. bias. The relatively fast dynamic response enables the device operation in a.c. modes. As the electrochemical reactions that may occur at the interfaces can be partially reversed when the bias is changed, a longer lifetime is expected when the devices operate in a.c. modes.

5. Conclusions

The photophysics of the pyridine-based systems is similar to that of PPV; however, the addition of (n,π^*) states into the electronic structure leads to interesting new behavior, such as a morphology-dependent intersystem crossing rate. An enhancement of intersystem crossing in powder samples has allowed us to resolve directly the production of triplet excitons in these polymers, and we conclude that the triplets are created directly from relaxed singlet excitons.

The reasonably high internal PL quantum efficiencies for these samples (about 10%) indicate that they should be good candidates for light-emitting device applications. The film samples show a tendency towards the formation of aggregate states, and it is possible that higher PL efficiencies may be achieved through control of aggregate formation. In particular, disordered samples (i.e. powders) do not appear to show aggregate formation.

We have successfully fabricated both LEDs and SCALE devices using PPy, PPyV, and copolymers of PPyV and PPV derivatives. The introduction of EB layers within SCALE devices significantly reduces the effective charge injection barrier, therefore enhancing the charge injection efficiency

from the electrodes to the emitting polymer. As a result, stable high workfunction metals, e.g. Au, can be used as charge injection electrodes, which may reduce the problems of aging of contacts of polymer light-emitting devices. As suggested by the important roles played by the interfaces in the device operation, the SCALE device structure is quite general. It can be applied to a variety of electroluminescent polymers in conjunction with suitable polymers to fabricate SCALE devices.

Dedication

This paper is dedicated to Esther M. Conwell, who has shown unfailing leadership in the field of electronic polymers. She has continuously challenged the electronic polymer community to produce the highest quality science. Her insights into electronic structure and charge transport have had a major impact on us and the electronic polymer community as a whole. We look forward to her continued influence and wish her the best for the future.

Acknowledgements

This work was supported in part by the Office of Naval Research and The Ohio State University Center for Materials Research.

References

[1] See, for example: *Proc. Int. Conf. Science and Technology of Synthetic Metals (ICSM '94), Seoul, Korea, 24–29 July 1994, Synth. Met., 69–71* (1995); *Proc. 2nd Int. Conf. Optical Probes of Conjugated Polymers and Fullerenes, Salt Lake City, UT, USA, 15–19 Feb. 1994, Mol. Cryst. Liq. Cryst., 256* (1994).

[2] T. Tamamoto, T. Ito and K. Kubota, *Chem. Lett.*, (1988) 153.

[3] M.J. Marsella, D.K. Fu and T.M. Swager, *Adv. Mater., 7* (1995) 145.

[4] D.K. Fu, B. Xu, M. Marsella and T.M. Swager, *Polym. Prepr., 36* (1995) 585.

[5] A.G. MacDiarmid and A.J. Epstein, *Faraday Discuss. Chem. Soc., 88* (1989) 317.

[6] Y.Z. Wang, D.D. Gebler, L.B. Lin, J.W. Blatchford, S.W. Jessen, H.L. Wang and A.J. Epstein, *Appl. Phys. Lett., 68* (1996) 894; Y.Z. Wang, D.D. Gebler, J.W. Blatchford, S.W. Jessen, L.B. Lin, T.L. Gustafson, H.-L. Wang, Y.W. Park, T.M. Swager, A.G. MacDiarmid and A.J. Epstein, *Proc. SPIE, 2528* (1995) 54.

[7] Y.N. Gartstein, M.J. Rice and E.M. Conwell, *Phys. Rev. B, 51* (1995) 1683.

[8] M. Chandross, S. Mazumdar, S. Jeglinski, X. Wei and Z.V. Vardeny, *Phys. Rev. B, 50* (1994) 14 702.

[9] M. El-Sayed, *J. Chem. Phys., 38* (1963) 2834.

[10] J.W. Blatchford, S.W. Jessen, L.B. Lin, J.J. Lih, T.L. Gustafson, A.J. Epstein, D.K. Fu, T.M. Swager, A.G. MacDiarmid, S. Yamaguchi and H. Hamaguchi, *Phys. Rev. Lett., 76* (1996) 1513; J.W. Blatchford, *Ph.D. Thesis*, The Ohio State University, 1996.

[11] J.W. Blatchford, S.W. Jessen, L.B. Lin, T.L. Gustafson, A.J. Epstein, D.K. Fu, H.L. Wang, T.M. Swager and A.G. MacDiarmid, in L.R. Dalton, A.K.-Y. Jen, G.E. Wnek, M.F. Rubner, C.Y.-C. Lee and L.Y. Chiang (eds.), *Electrical, Optical and Magnetic Properties of Organic Solid State Materials III*, Materials Research Society, Pittsburgh, 1996, in press.

[12] U. Lemmer, S. Heun, R.F. Mahrt, U. Scherf, M. Hopmeier, U. Siegner, E.O. Gobel, K. Mullen and H. Bassler, *Chem. Phys. Lett., 240* (1995) 373.

[13] S.W. Jessen, J.W. Blatchford, L.B. Lin, T.L. Gustafson, A.J. Epstein, D.K. Fu, T.M. Swager, A.G. MacDiarmid, T. Yuzawa and H. Hamaguchi, submitted for publication.

[14] J.W. Blatchford, A.J. Epstein, P.F. Barbara, T.M. Swager and A.G. MacDiarmid, unpublished results.

[15] M. Yan, L.J. Rothberg, F. Papadimitrakopoulos, M.E. Galvin and T.M. Miller, *Phys. Rev. Lett., 72* (1994) 1104.

[16] K. Yoshihara, A. Namiki, M. Sumitani and N. Nakashima, *J. Chem. Phys., 71* (1979) 2892.

[17] S.W. Jessen, A.J. Epstein and J. Shinar, unpublished results.

[18] G.S. Kanner, X. Wei, B.C. Hess, L.R. Chen and Z.V. Vardeny, *Phys. Rev. Lett., 69* (1992) 538.

[19] J.M. Leng, S. Jeglinski, X. Wei, R.E. Benner, Z.V. Vardeny, F. Guo and S. Mazumdar, *Phys. Rev. Lett., 72* (1994) 1104.

[20] J.H. Burroughes, D.D.C. Bradley, A.R. Brown, R.N. Marks, K. Mackay, R.H. Friend, P.L. Burn and A.B. Holmes, *Nature, 347* (1990) 539.

[21] D.C. Bradley, *Synth. Met., 54* (1993) 401.

[22] J. Kido, *Trends Polym. Sci., 2* (1994) 350.

[23] I.D. Parker, *J. Appl. Phys., 75* (1994) 1656.

[24] D.D. Gebler, Y.Z. Wang, J.W. Blatchford, S.W. Jessen, L.B. Lin, T.L. Gustafson, H.L. Wang, T.M. Swager, A.G. MacDiarmid and A.J. Epstein, *J. Appl. Phys., 78* (1995) 4264; H.L. Wang, M.J. Marsella, D.K. Fu, T.M. Swager, A.G. MacDiarmid and A.J. Epstein, *Polym. Mater. Sci. Eng., 73* (1995) 473.

[25] M.A. Lampert and P. Mark, *Current Injection in Solids*, Academic Press, New York, 1970.

[26] Y.Z. Wang et al., unpublished results.

[27] F. Garten, A.R. Schlatmann, R.E. Gill, J. Vrijmoeth, T.M. Klapwijk and G. Hadziioannou, *Appl. Phys. Lett., 66* (1995) 2540.

[28] S.A. Jeglinski, M.E. Hollier, J. Gold, Z.V. Vardeny, Y. Ding and T. Barton, *Mol. Cryst. Liq. Cryst., 256* (1994) 555.

[29] Z. Yang, B. Hu and F.E. Karasz, *Macromolecules, 28* (1995) 6151.

[30] A.C. Fou, O. Onitsuka, M. Ferreira, D. Howie and M.F. Rubner, *Polym. Mater. Sci. Eng., 72* (1995) 160.

[31] H.K. Henisch, *Semiconductor Contacts, An Approach to Ideas and Models*, Oxford University Press, London, 1984.

[32] E.H. Rhoderick and R.H. Williams, *Metal–Semiconductor Contacts*, Oxford University Press, London, 1988.

[33] A.G. MacDiarmid, H.L. Wang, J.W. Park, D.K. Fu, M.J. Marsella, T.M. Swager, Y.Z. Wang, D.D. Gebler and A.J. Epstein, *Proc. SPIE, 2528* (1995) 2.

[34] Y. Yang, E. Westerweele, C. Zhang, P. Smith and A.J. Heeger, *J. Appl. Phys., 77* (1995) 694.